

# Large scale numerical simulations of “ultrametric” long-range depinning

Damien Vandembroucq and Stéphane Roux  
*Unité Mixte CNRS/Saint-Gobain “Surface du Verre et Interfaces”  
39 Quai Lucien Lefranc, 93303 Aubervilliers cedex, FRANCE*

The depinning of an elastic line interacting with a quenched disorder is studied for long range interactions, applicable to crack propagation or wetting. An ultra-metric distance is introduced instead of the Euclidean distance, allowing for a drastic reduction of the numerical complexity of the problem. Based on large scale simulations, two to three orders of magnitude larger than previously considered, we obtain a very precise determination of critical exponents which are shown to be indistinguishable from their Euclidean metric counterparts. Moreover the scaling functions are shown to be unchanged. The choice of an ultrametric distance thus does not affect the universality class of the depinning transition and opens the way to an analytic real space renormalization group approach.

## I. INTRODUCTION

The depinning of an elastic interface in a random environment gives a common theoretical framework to describe physical phenomena as various as the advance of a magnetic wall, the propagation of a fracture front or the wetting of a disordered surface (see *e.g.* Ref. [1, 2, 3] for a recent review). The richness of the physics encountered in these different situations results from the same feature. The disorder of the environment which tends to anchor the interface competes with an elastic-like term which tends to keep the interface smooth. The tuning of an external driving force allows to go through a critical transition. Below threshold the interface can only advance over a finite distance before stopping in a blocked conformation. Above threshold the interface can move freely and acquire a finite velocity. At threshold the system is characterized by a set of universal critical exponents.

In the case of over-damped dynamics the motion can be described by the following stochastic equation:

$$\mu\partial_t h(x,t) = F_{ext}(t) + F_{el}(x,t) + \gamma[x, h(x,t)] \quad (1)$$

where  $h(x,t)$  denotes the position of the front,  $F_{ext}(t)$  the external driving force,  $F_{el}(x,t)$  the elastic term due to the distortion of the front and  $\gamma[x, h(x,t)]$  the frozen disorder. Depending on the physical phenomenon considered the elastic term can take different forms. In the case of magnetic walls or of wetting in a Hele-Shaw cell, the interactions to be taken into account are short ranged and at first order the elastic force can be estimated by a simple Laplacian term:  $F_{el}(x,t) = \nabla^2 h(x,t)$ . In the case of the advance or receding of a triple line on a disordered substrate [4] or of the propagation of fracture front long range interactions have to be considered. In the latter case elastic interactions are mediated *via* the bulk along the whole front. A first order perturbation analysis for the front roughness gives[5]:

$$F_{el}(x,t) = \frac{1}{\pi} \int dx' \frac{h(x,t) - h(x',t)}{|x - x'|^2} \quad (2)$$

This long range elastic string model has been widely studied over the last ten years. In particular the interface is shown to exhibit a self-affine roughness: the width  $w$  of the interface scales with the system size  $L$  as  $w \propto L^\zeta$ . The different numerical works [6, 7, 8, 9] performed give estimations of the roughness exponent  $\zeta$  spreading in the interval [0.34 – 0.40]. The latter exponent and more generally the universality class of the model depend strongly on the long range nature of the kernel in Eq. (2). For instance, if  $F_{el} \propto \nabla^2 h$ , then  $\zeta = 1.25$ . The most recent results obtained by Rosso and Krauth [7] give a value  $\zeta \approx 0.39$  significantly larger than the theoretical prediction  $\zeta = 1/3$  obtained by one-loop calculations of renormalization group technique[10, 11] and equally smaller than the recent two-loop estimation[12]  $\zeta \approx 0.47$ . Note however that these values are not consistent with the results  $\zeta \approx 0.5 - 0.6$  obtained experimentally for interfacial fracture[9] or wetting[13, 14]. Therefore it is of utmost importance to have an accurate determination of these critical exponents, and thus to be able to study large system sizes.

In the following we present an ultrametric version of an extremal model of depinning (see Ref. [8] for a detailed study of the original model with Euclidean metric). The complexity of the elementary step of calculation is shown to scale with the system size  $L$  as  $\log_2 L$  instead of  $L$  in the original model. This allows us to perform simulations on systems of size  $L = 2^{20} \approx 10^6$ , which corresponds to a gain of two to three orders of magnitude compared with other published works based on the Euclidean metrics. The universality class of the model is shown to be unchanged. Beyond the numerical acceleration, this ultrametric model of depinning may thus also serve as a starting point for a real space renormalization analysis.

The paper is organized as follows: In a first part we recall the definition of the original model, we then define the ultrametric version and present the main features of the new model. In the second part we give results of simulations performed on large systems and focus on the critical properties of this ultrametric model of depinning. We conclude that it lies in the same universality class as its euclidean version. The details of the numerical implementation of the algorithm are finally given in an

appendix.

## II. EXTREMAL DRIVING OF A DEPINNING FRONT

Various numerical techniques can be used to study the depinning phenomenon in the vicinity of the critical threshold. Early works used a direct integration of the equation above *via* Euler[6] or Runge-Kutta [15] schemes. Recently Rosso and Krauth [7] developed an iterative algorithm to determine the blocked conformations corresponding to a given constant forcing. They used periodic boundary conditions both along the front and in the direction of propagation and the critical threshold is reached when the last blocked conformation starts moving.

In the case of strong pinning the advance of the front proceeds by successive local instabilities. This avalanche behavior is characteristic of the motion of a depinning front. This property can be exploited to develop an efficient algorithm describing the motion of the front close to the critical threshold. Instead of driving the front at a constant external force, it consists of tuning the latter at the exact value such that one and only one site can depin at a time. So doing, the sequence of depinning events is preserved. The implementation of this extremal dynamics which has been used since 1992 in various interface growth models [16, 17, 18, 19, 20, 21] is straightforward. At each iteration step one needs to identify the weakest site, to advance it up to the next trap and to update the long range elastic forces due to the change of front conformation. The latter operation scales with the size of the front. The great advantage of this method is that the system remain constantly at the edge of the critical behavior and it is not necessary to tune the external driving force (see *e.g.* Ref. [22] for a discussion on the use of extremal dynamics to reach the critical state and more generally on the link between Self Organized Criticality and classical critical transitions).

Based on the above described extremal modeling, we now detail the way to implement the model numerically. The front is discretized along a regular horizontal grid;  $i \in [0, L - 1]$  and  $h_i$  are the coordinates along the front and in the direction of propagation respectively. Traps of random depths  $\gamma_i$  are randomly distributed along the direction of propagation. The distortion of the front induces elastic forces  $f_i^{el}$  *via* a Green function  $G_{ij} = G(r_{ij})$  where  $r_{ij}$  is the euclidean distance separating two sites  $i$  and  $j$  along the front. In the case of a fracture front, a discretized version of the elastic redistribution function is such that

$$G_{ij} \propto_{i \neq j} |i - j|^{-2}, \quad G_{ii} = - \sum_{i \neq j} G_{ij}. \quad (3)$$

Let us consider a given conformation of the front. For each site  $(i, h_i)$  located in a trap of depth  $\gamma_i$ , we can define a local depinning threshold  $s_i = \gamma_i - f_i^{el}$ : this site

depins as soon as the external driving force  $F$  overcomes the threshold  $F > s_i$ . The depinning threshold  $s(t)$  of the front conformation obtained at iteration  $t$  thus corresponds to the minimal external force to be exerted so that at least one site of the front can depin:  $s(t) = \min_i s_i$ . Finally the critical threshold  $s^*$  above which the front can freely propagate is  $s^* = \max_t s(t)$ . The basic rule of the extremal driving consists simply at each iteration step  $t$  of simply tuning the external force at exactly the value of the depinning threshold of the current front conformation:  $F(t) = s(t)$ . Once identified, the extremal site is advanced up to the next trap, the elastic forces are updated to take into account this local displacement and the new value  $s(t + 1)$  of the front depinning threshold is evaluated. We summarize below the elementary steps of the algorithm used to run the model and we estimate their complexity respectively to the size  $L$  of the system.

- A** initialization  $h_i \leftarrow 0, f_i^{el} \leftarrow 0, \gamma_i \leftarrow rnd$  [L]  
 $i \in [0 - L], L = 2^n$
- B** identification of the extremal site  $i_0$  [L]  
such that  $\gamma_{i_0} - F_{i_0} = \min_i (\gamma_i - f_i^{el})$
- C** advance of the extremal site [1]  
 $\delta h_{i_0} \leftarrow rnd, h_{i_0} \leftarrow h_{i_0} + \delta h_{i_0}$
- D** update of the trap depth  $\gamma_{i_0} \leftarrow rnd$  [1]
- E** update of the elastic forces  $f_i^{el} \leftarrow f_i^{el} + G_{ii_0} \delta h_{i_0}$  [L]  
where  $G_{ij} \propto |i - j|^{-2}$
- F** back to step B

where  $rnd$  stands for a random number and  $a \leftarrow b$  for the assignment of value  $b$  to variable  $a$ . Except the first initialization step, the two limiting steps are the identification of the extremal site and the update of elastic forces along the front which both scale linearly with the system size  $L$ . This sequence of elementary steps is then iterated  $T$  times to obtain statistical averages of the quantities of interest.

## III. ULTRAMETRIC DEPINNING

We now turn to the presentation of the ultrametric model. The basic rules of the extremal model remain identical but the redistribution of the elastic forces. Instead of using the natural euclidean distance along the front we use an ultrametric distance. The structure of the algorithm stays roughly similar to the previous one but steps **B** and **E** are shown to be characterized by a complexity in  $\log_2 L$  instead of  $L$ .

The most natural structure to be used in the context of a model with ultrametric distance is a dyadic tree. Let us first build such a tree whose final leaves are the  $L$  sites of the depinning front. As illustrated on Fig. 1, the simplest ultrametric distance between two sites  $i$  and  $j$  is the number of branches that composes the shortest path on the tree between the two sites. This is exactly twice the depth  $m$  of the nearest common ancestor of these two

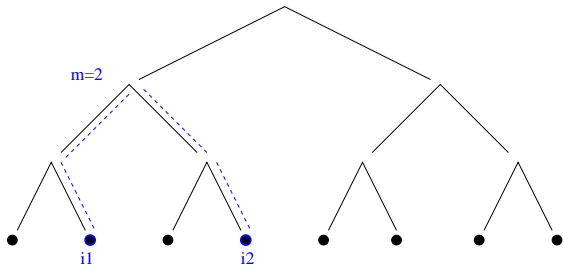


FIG. 1: The depth  $m$  of the first common ancestor of sites  $i_1$  and  $i_2$  is used to compute the ultrametric distance between points  $i_1$  and  $i_2$  as  $d_u(i_1, i_2) = 2^m - 1$

sites. Different choices of distance are possible based on the tree structure. In the following we use a definition that preserves the scaling of the Euclidean distance:

$$d_u(i, j) = 2^m - 1 \quad (4)$$

An important characteristic of this ultrametric distance is its degeneracy. Namely there is one point at distance  $d = 2^1 - 1 = 1$ , two points at distance  $d = 2^2 - 1 = 3$  and  $2^{p-1}$  points at distance  $d = 2^p - 1$ . For a set of  $L = 2^n$  points one thus counts only  $n = \log_2 L$  different values for the distance between two points of the set. There lies the main advantage of the choice of an ultrametric distance from the computational complexity point of view. The expression of the elastic Green function then derives directly from the definition of the new distance:

$$G_{ij} = G[d_u(i, j)] \propto \frac{1}{d_u(i, j)^2} \quad (5)$$

$$G_{ii} = - \sum_{m=1}^{\log_2 L} 2^{m-1} G[2^m - 1]$$

Using this definition, we can easily accelerate the update of elastic forces (step E). As illustrated on Fig. 2 instead of updating  $L$  sites, we can update only  $\log_2 L$  subtrees corresponding to sites located at the same ultrametric distance of the extremal site. A similar gain can be obtained on step B for the determination of the extremal site. Technical details regarding the numerical implementation of the algorithm are developed in the appendix. The basic steps of the algorithm then scale with  $\log_2 L$  instead of  $L$ . The price to pay for this numerical advantage is the loss of the translational invariance. We show below that it does not affect the universality class of the model.

The simulations have been performed on systems of sizes up to  $L = 2^{20}$ . The numerical runs were performed over a large duration  $T$  respective to the natural correlation time of the system  $\tau_L \propto L^z$ . In the case of the largest system  $L = 2^{20}$  we used  $T = 2.510^{10} \approx 100\tau_L$ .

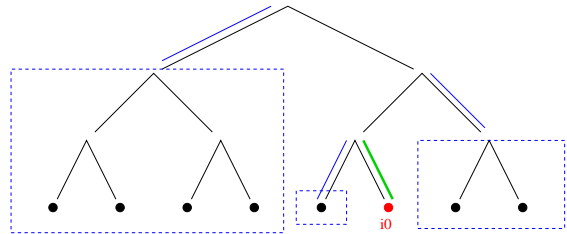


FIG. 2: When redistributing elastic forces after the depinning of the extremal site  $i_0$ , all sites located at the same ultrametric distance  $m = d_u(i, i_0)$  belong to a common subtree and receive the same contribution. This allows an update by block that scales with the number  $\log_2 L$  of these subtrees. Similarly the tree structure allows to find the next extremal sites in only  $\log_2 L$  operations.

#### IV. CHARACTERIZATION OF THE CRITICAL STATE: NUMERICAL RESULTS

The propagation of depinning fronts at the critical threshold exhibits a rich phenomenology. The front presents a self-affine roughness: its width  $w(\Delta x)$  measured over a distance  $\Delta x$  scales as  $w(\Delta x) \propto \Delta x^\zeta$ , where  $\zeta$  is the roughness exponent.

The dynamics of depinning is characterized by an avalanche behavior. In the framework of an extremal dynamics this can be described by the distribution of the distances  $r$  between two successive depinning sites:  $P(r) \propto r^{-a}$ . Generalizing this distribution for sites corresponding to depinning events separated by a given time lag allows to obtain in addition the dynamic exponent  $z$  which characterizes the spreading of the avalanches. Namely the lateral extension  $\xi$  of an avalanche of duration  $\Delta t$  scales as  $\xi \propto \Delta t^{1/z}$ .

Another quantity of interest is the external force  $s$  needed to depin a given conformation of the front. It can be shown [23, 24] that the distribution  $\mathcal{Q}(s)$  of these front depinning forces exhibits a singular behavior close to the critical threshold  $s^*$ :  $\mathcal{Q}(s) \propto (s^* - s)^\mu$ .

In the following we present simulations of ultrametric depinning performed on large systems (up to  $L = 2^{20}$ ). We recover all critical features described above with exponents numerically indistinguishable from their counterparts in the Euclidean version of the model.

##### A. Self-affine roughness

Various statistical roughness estimators can be used to characterize the self-affine properties of a rough front. Consider for example the standard deviation  $\sigma(\Delta x)$  of the height differences between points separated by a distance  $\Delta x$ . A self-affine front obeys  $\sigma(\Delta x) \propto \Delta x^\zeta$ . Similarly the width  $w(L)$  of a front of length  $L$  (*i.e.* the standard deviation of the height distribution along the front) scales as  $w(L) \propto L^\zeta$ . Fourier or wavelet transforms are also of standard use.

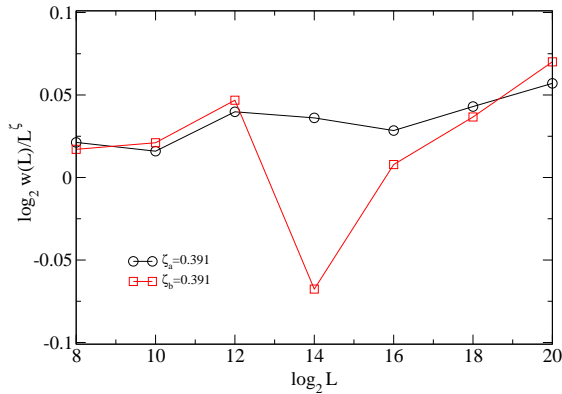


FIG. 3: Width  $w(L)$  of the front (standard deviation of the height distribution) for growing lateral sizes  $L$  after normalization by a power law of exponent  $\zeta$ . The simulations have been run from over  $100 \times 10^6$  iterations steps for  $L = 2^8$  up to  $25 \times 10^9$  for  $L = 2^{20}$ . The circle and the square symbols correspond respectively to a uniform and a Gaussian distribution of the trap depth.

In the context of this study we can also design a “wavelet like” roughness estimator which exploits the natural tree structure associated to the ultrametric distance. At the level  $\ell = n = \log_2 L$  we define  $\omega^2(n)$  as the variance of the height difference between nearest neighbors:

$$\omega^2(n) = \left\langle (h_i - h_j)^2 \right\rangle_{d_u(i,j)=2^n-1} \quad (6)$$

At the upper level the height of a node is thus simply defined as the arithmetic average of its two ancestors:  $h^{(\ell-1)}(i) = [h^{(\ell)}(2i) - h^{(\ell)}(2i+1)]/2$  and the corresponding variance  $w(m)$  is computed. This sequence is iterated up to the root of the tree. At each level  $m$  corresponds an ultrametric distance  $m = n - \ell + 1$  and we have

$$\omega^2(m) \propto 2^{2\zeta(m-1)}, \quad \text{or} \quad \omega(m) \propto d_u(m)^\zeta \quad (7)$$

We present now numerical results obtained for these various roughness estimators. The simulations have been performed on systems of sizes up to  $L = 2^{20}$ . In Fig. 3 and 4 we show the scaling behaviors obtained for the wavelet roughness estimator  $\omega(d_u)$  and the width  $w(L)$  of the interface. We obtain perfect power law behaviors over six decades and we only show here in logarithmic scale the residuals after normalization by a power law of exponent  $\zeta$ . This procedure is a very sensitive way of detecting deviations from a power law. Note that previous published works deal with  $\log_2 L \leq 10$ .

We present simulations performed with two kinds of distributions for the trap depths, uniform and Gaussian (respectively denoted by the subscripts  $a$  and  $b$  in the figures).

An estimation of the roughness exponent can be extracted from each individual set of data. Note that

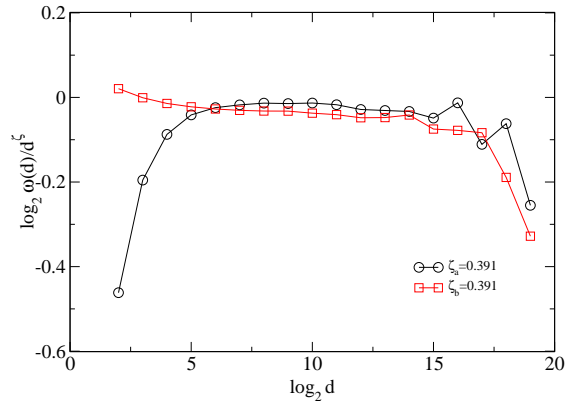


FIG. 4: Wavelet roughness estimator  $\omega(m)$  against the ultrametric distance  $d_u(m) = 2^m - 1$ . The simulations have been performed on a system of size  $L = 2^{20}$  run over  $25 \times 10^9$  iteration steps. The circle and the square symbols correspond respectively to a uniform and a Gaussian distribution of the trap depth.

the fluctuations of this estimate due to the choice of the nature of disorder or the roughness estimator are larger than the deviation from the power law behavior itself. All results are presented here with the central value  $\zeta = 0.391$ . This value slightly underestimates the results obtained from the width estimator and slightly overestimates the results obtained from the wavelet estimator. A conservative estimate of the roughness exponent thus appears to be:

$$\zeta = 0.391 \pm 0.005 \quad (8)$$

## B. Avalanche behavior – Dynamic exponent

The avalanche behavior is characteristic of the dynamics of the front close to threshold forcing. Although an extremal driving does not allow to recover the real dynamics of the front, avalanches associated to a given level of the driving force  $F$  can be reconstructed from the history of the extremal force signal  $s(t)$ . An avalanche thus consists of a continuous series of depinning events such that  $s(t) < F$ . Instead of reconstructing these avalanches it is classical in the framework of extremal models [25] to work directly from the extremal force signal. Let us consider a time lag  $\Delta t$  (a number of iterations), we introduce the distance  $\Delta x$  along the front between the sites depinning at  $t$  and  $t + \Delta t$  respectively. It appears [8] that the distributions of these distances  $\Delta x$  at fixed time lag  $\Delta t$  can be rescaled on a universal form:

$$P(\Delta x; \Delta t) = \frac{1}{\Delta x^a} \psi \left( \frac{\Delta x}{\Delta t^{1/z}} \right) \quad (9)$$

where  $\psi(u) \propto u^a$  for  $u \ll 1$  and  $\psi(u) \approx \text{cste}$  for  $u \gg 1$ . The exponent  $a$  is well approximated by the exponent of

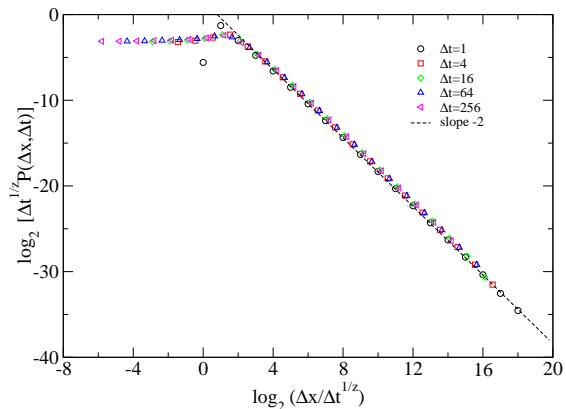


FIG. 5: After rescaling the distribution of ultrametric distances  $d_u$  between sites depinning at time  $t$  and  $t + \Delta t$  collapse on a unique master curve. The dynamic exponent used for the rescaling is  $z = 1.39$ .

elastic kernel of Eq. (2)  $a \approx 2$  and the dynamic exponent  $z$  can be related to the roughness exponent: if a sequence of  $\Delta t$  depinning events spreads over a distance  $\Delta x$  along the front, the knowledge of the roughness of the front over  $\Delta x$  leads to  $\Delta t \approx \Delta x \Delta x^\zeta$  thus  $z = 1 + \zeta$ [8, 26].

This scaling is recovered in the framework of ultrametric depinning, where we measured  $P(d_u, \Delta t)$ . We check on Fig. 5 that after rescaling all distributions collapse on a unique master curve. The rescaling was obtained with the value  $z = 1.39$ , for large arguments the behavior of  $\psi$  is well approximated by a power law of exponent  $a = 2$ .

## V. SCALING FUNCTIONS

In addition to critical exponents, the pinned state is also characterized by scaling functions[27]. In the specific case of interface dynamics, this means that the critical properties of the front are described by a universal exponent and a universal function describing the fluctuations of the (rescaled) width of the interface. This property has been evidenced for various growth models (Edwards-Wilkinson, Kardar-Parisi-Zhang...)[27] and has been recently applied to the case of depinning interfaces [28]. Note that in the latter case, beyond the interface width, the technique can be used to characterize other fluctuating quantities. In particular, the distribution of the depinning threshold of a finite elastic line under extremal driving can be shown to be universal[23, 29]. In the present study we show that the choice of an ultrametric distance does not affect these universal distributions. More precisely the fluctuations of interface width and depinning threshold are shown to be described by universal functions and these functions appear to be very close to or identical to their counterparts obtained in the framework of a depinning model with Euclidean distance.

These statistical distributions are however sensitive to

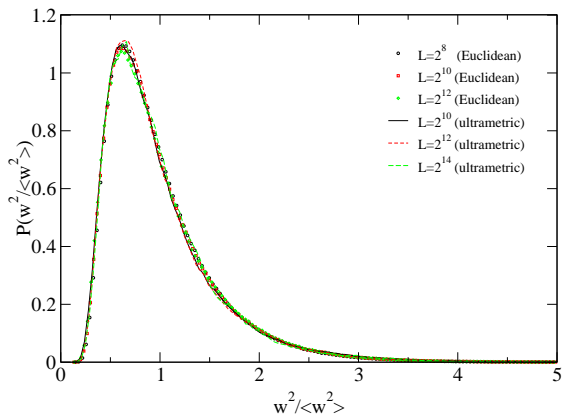


FIG. 6: Distribution of the rescaled width of the depinning front for sizes  $L = 2^{10}$ ,  $2^{11}$  and  $L = 2^{12}$  in the Euclidean model and  $L = 2^{10}$ ,  $2^{12}$  and  $L = 2^{14}$  in the ultrametric model. All distributions collapse on the same curve.

the boundary conditions (periodic boundary conditions *vs* isolated system)[30]. In the following we use periodic boundary conditions. In the ultrametric case the resummation over all replicas induces an additional mean field contribution  $1/2L^2$  equally shared by all  $G_{ij}$ ,  $i \neq j$ .

### A. Universal width fluctuations

Following Ref. [28] we study the distribution of the rescaled width  $w^2 / \langle w^2 \rangle$  where  $\langle w^2 \rangle$  is the temporal average of the width of a depinning front of finite extent  $L$ . In Fig. 6 we present results obtained for various system sizes in both cases of Euclidean and ultrametric distance. We observe that all rescaled distributions collapse onto a master curve whatever the size of the front and the Euclidean or hierarchical metric.

### B. Universal depinning force fluctuations

As developed above, the extremal dynamics gives a direct access to the fluctuations of the driving force needed to depin the front site by site. Most of these fluctuations simply correspond to the depinning of near neighbors (which receive the largest contributions of the elastic redistribution) and are highly sensitive to the details of the pinning force disorder. The other part of these fluctuations corresponds to depinning events taking place at a larger distance  $d$  from the previous depinning site. In other terms, the front can be regarded as pinned over the distance  $d$  between the two successive extremal sites. Conditioning the depinning force distribution to this distance  $d$  between successive extremal sites thus allows to define distributions of size dependent effective thresholds. (Note that in the context of fracture, it can be seen as a distribution of effective toughness[31]). An effective

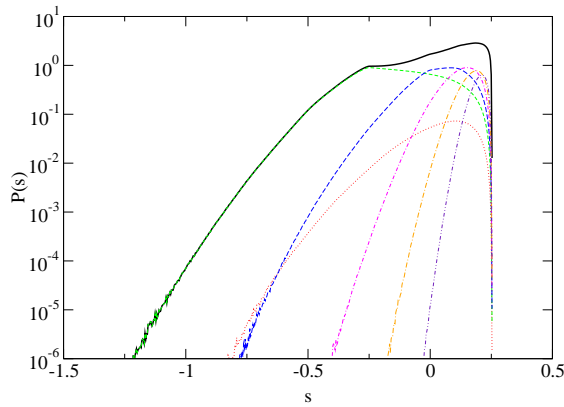


FIG. 7: Distribution of depinning forces (bold line) and contributions corresponding to growing distances along the front between successive depinning sites. The larger the distance the narrower the distribution and the closer from the critical threshold  $s^*$ .

threshold over a distance  $d$  can also be seen as the force needed to entirely depin a front of size  $d$ . It can actually be shown [23, 29] that as  $d$  increases, the distributions  $P(s; d)$  tend to peak and approach the critical threshold  $s^*$ . This behavior is recovered in our ultrametric variant as illustrated on Fig. 7 where we plotted the global distribution  $P(s)$  and the contributions  $P(s; d_u)$  corresponding to the different ultrametric distances.

The typical elastic force fluctuations over a distance  $d$  can moreover be estimated:  $\delta f^{el} \propto d^{-(1-\zeta)}$ . Both the width  $\sigma_s(d)$  and the gap to the critical threshold  $\delta_s(d) = s^* - \langle s \rangle(d)$  of the center of these distribution actually follow this scaling. As developed in Ref. [23, 29] this property allows for a precise extrapolation of the critical threshold by extrapolation of the linear relationship between  $\langle s \rangle(d)$  and  $\sigma_s(d)$  up to the force value canceling  $\sigma_s$ . Moreover this rescaling results in a collapse of all distribution over a single master curve:

$$P(s; d) = d^{1-\zeta} \chi [d^{1-\zeta}(s^* - s)]. \quad (10)$$

We see on Fig. 8 that the choice of an ultrametric distance slightly changes the shape of the distribution obtained after rescaling. This may mean that these conditional distributions are more sensitive to the boundary conditions and the loss of translation invariance induced by the ultrametric model than a macroscopic quantity such as the width of the interface.

## VI. CONCLUSION

We developed a depinning model based on the use of an ultrametric distance. This choice allows to reduce the complexity of an elementary step of computation to  $\log_2 L$  with respect to the system size  $L$ . We performed

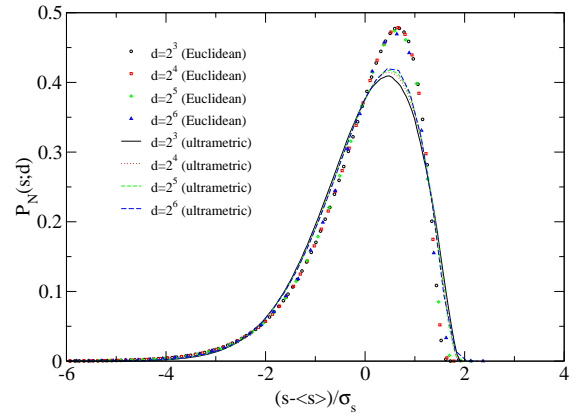


FIG. 8: After renormalization the centered unit conditional distribution of depinning force fall onto a single curve independently of the length  $d$ . The master curve obtained in the ultrametric case (continuous lines) slightly differ from its Euclidean counterpart (symbols).

numerical simulations on systems of size  $10^6$  more than two orders of magnitude larger than in previously published results. We propose an estimate of the roughness exponent  $\zeta = 0.390 \pm 0.01$  consistent with the values measured for the Euclidean counterpart of the model. Moreover we obtained scaling functions either identical or very close in both cases. Therefore the choice of an ultrametric distance appears not to affect the universality class of the depinning transition.

Beyond the numerical efficiency, this model may thus serve as a starting point for a real space renormalization analysis. Indeed a coarse grained picture of the model preserves exactly the same structure with “dressed” thresholds and front advances, and thus the solution of a simple  $L = 2$  front model may open the way to an analytic determination of critical exponents and universal scaling functions.

## APPENDIX A: NUMERICAL IMPLEMENTATION OF THE MODEL

In this appendix we describe the algorithm used to run this ultrametric model of depinning. As above mentioned the structure of the algorithm is roughly similar to the original one but steps **B** and **E** are characterized by a complexity in  $\log_2 L$  instead of  $L$ .

Let us first consider the redistribution of elastic forces that take place after a depinning event. The increment of force at a given site  $j$  only depends on its distance  $d_u(i_0, j) = 2^m - 1$  to the extremal site  $i_0$ . Actually  $2^{m-1}$  different sites are at this same distance from the extremal site  $i_0$  and form a subtree (see Fig. 2). Instead of updating sequentially the elastic force increment on every sites it is possible to update the elastic force acting on the whole subtree. To this aim we define the force  $\varphi_{i,\ell}^{el}$

as the force transported by the  $i^{\text{th}}$  branch of the  $\ell^{\text{th}}$  level of the tree. The first level ( $\ell = 1$ ) here corresponds to the two branches at the root and the level ( $\ell = \log_2 L$ ) to the branches pointing toward the  $L$  sites of the front (the leaves of the tree). Using this definition the elastic force acting on site  $i$  is nothing but the sum of the forces transported by its ancestor branches:

$$f_i^{el} = \sum_{\ell=1}^{n=\log_2 L} \varphi_{\frac{i}{2^{n-\ell}}, \ell}^{el} \quad (\text{A1})$$

In the hierarchical algorithm the step **E** thus consists of updating the branches of the force tree affected by the redistribution of elastic forces :  $\varphi_{j_0, \ell}^{el} = \varphi_{j_0, \ell}^{el} + G_{i_0, m} \delta h_{i_0}$ ,  $j_0 = \{i_0/2^{n-\ell}\}$  where  $\{i\}$  is the operation of exchanging the parity bit of  $i$ .

In the same spirit we can build a tree to determine the value and location of the extremal site. The determination of the extremal site requires *a priori*  $L-1$  operations of elementary comparisons to find  $s^* = \min_i(\gamma_i - f_i^{el})$ . After each depinning event, the elastic forces are updated on every sites so that the same  $L-1$  operations have to be performed at each iteration. In the ultrametric model the situation is slightly different because the elastic force on a site can be written as a sum of the forces transmitted by the branches of the tree (see Eq. A1). As a consequence two sites  $i$  and  $j$  share all force components acting on branches above their nearest common ancestor.

$$f_i^{el} = \Phi_m + \sum_{\ell=m+1}^{n=\log_2 L} \varphi_{\frac{i}{2^{n-\ell}}, \ell}^{el} \quad (\text{A2})$$

$$f_j^{el} = \Phi_m + \sum_{\ell=m+1}^{n=\log_2 L} \varphi_{\frac{j}{2^{n-\ell}}, \ell}^{el} \quad (\text{A3})$$

$$\Phi_m = \sum_{\ell=1}^m \varphi_{\frac{i}{2^{n-\ell}}, \ell}^{el} = \sum_{\ell=1}^m \varphi_{\frac{j}{2^{n-\ell}}, \ell}^{el} \quad (\text{A4})$$

We can then perform the comparison operations level by level going up the tree of elastic forces. To be more specific let us define the following hierarchical structure. At level  $n = \log_2 L$  we define

$$\sigma_{i, n} = \gamma_i, \quad \alpha_{i, n} = i \quad (\text{A5})$$

then we proceed iteratively up to the root of the tree:

$$\sigma_{i, p-1} = \min(\sigma_{2i, p} + \varphi_{2i, p}^{el}, \sigma_{2i+1, p} + \varphi_{2i+1, p}^{el}) \quad (\text{A6})$$

$$\begin{aligned} \alpha_{i, p-1} &= \alpha_{2i, p} && \text{if } \sigma_{2i, p} + \varphi_{2i, p}^{el} < \sigma_{2i+1, p} + \varphi_{2i+1, p}^{el} \\ &= \alpha_{2i+1, p} && \text{if } \sigma_{2i, p} + \varphi_{2i, p}^{el} > \sigma_{2i+1, p} + \varphi_{2i+1, p}^{el} \end{aligned} \quad (\text{A7})$$

The location and the value of the extremal site are thus given by

$$s^* = \sigma_{1, 0}, \quad i_0 = \alpha_{1, 0} \quad (\text{A8})$$

Without prior knowledge, the computation for the determination of the extremal site of a given conformation is simply the sum of all comparisons at each level of the tree:  $\sum_1^n 2^{p-1} = 2^n - 1 = L - 1$ . This is exactly the same result as in the standard case. Consider now the situation after the depinning event: the trap depth  $t_{i_0}$  is updated at the extremal site and only  $n = \log_2 L$  branches of the tree are altered by the elastic force distribution. A sequence of  $n$  comparisons thus allows to find the new extremal site: we start at the former extremal site  $i_0$ ,

$$p = n : j_0 = i_0, \sigma_{j_0} = t_{j_0}, \alpha_{j_0} = i_0 \quad (\text{A9})$$

then for  $p = n$  to  $p = 1$  we proceed iteratively to update the tree and determine the value  $\sigma_{1, 0}$  and location  $\alpha_{1, 0}$  of the new extremal site.

$$j_p = j_0/2^{n-p}, \quad k_p = \{j_p\} \quad (\text{A10})$$

$$\sigma_{j_{p-1}, p-1} = \min[\sigma_{j_p, p} + \varphi_{j_p, p}^{el}, \sigma_{k_p, p} + \varphi_{k_p, p}^{el}] \quad (\text{A11})$$

$$\begin{aligned} \alpha_{j_{p-1}, p-1} &= \alpha_{j_p, p} && \text{if } \sigma_{j_{p-1}, p-1} = \sigma_{j_p, p} \\ &= \alpha_{k_p, p} && \text{if } \sigma_{j_{p-1}, p-1} = \sigma_{k_p, p} \end{aligned} \quad (\text{A12})$$

---

[1] M. Kardar, Phys. Rep. **301**, 85 (1998).  
[2] H. Leschhorn, T. Nattermann, S. Stepanow, and L.-H. Tang, Ann. Phys. (Leipzig) **6**, 1 (1997).  
[3] D.-S. Fisher, Phys. Rep. **301**, 113 (1998).  
[4] J.-F. Joanny and P. de Gennes, J. Chem. Phys. **81**, 552 (1984).  
[5] H. Gao and J. Rice, J. Appl. Mech. **56**, 828 (1989).  
[6] M. Dong, M. Marchetti, A. Middleton, and V. Vinokur,

Phys. Rev. Lett. **70**, 662 (1993).  
[7] A. Rosso and W. Krauth, Phys. Rev. E **65**, 025101(R) (2002).  
[8] A. Tanguy, M. Gounelle, and S. Roux, Phys. Rev. E **58**, 1577 (1998).  
[9] K. Måløy and J. Schmittbuhl, Phys. Rev. Lett. **78**, 3888 (1997).  
[10] O. Narayan and D. Fisher, Phys. Rev. B **48**, 7030 (1993).

- [11] D. Ertas and M. Kardar, Phys. Rev. E **49**, R352 (1994).
- [12] P. Chauve, P. L. Doussal, and K. Wiese, Phys. Rev. Lett. **86**, 1785 (2001).
- [13] A. Prevost, E. Rolley, and C. Guthmann, Phys. Rev. Lett. **83**, 348 (1999).
- [14] S. Moulinet, C. Guthmann, and E. Rolley, Eur. Phys. J. E **8**, 437 (2002).
- [15] S. Zapperi, H. Herrmann, and S. Roux, Eur. Phys. J. B **17**, 131 (2000).
- [16] S. Zaitsev, Physica A **189**, 411 (1992).
- [17] K. Sneppen, Phys. Rev. Lett. **69**, 3539 (1992).
- [18] P. Bak and K. Sneppen, Phys. Rev. L **71**, 4083 (1993).
- [19] H. Leschhorn and L.-H. Tang, Phys. Rev. E **49**, 1238 (1994).
- [20] S. Roux and A. Hansen, J. Phys. I **4**, 515 (1994).
- [21] M. Paczuski, S. Maslov, and P. Bak, Phys. Rev. Lett. **74**, 4253 (1995).
- [22] R. Dickman, M. A. Muñoz, A. Vespignani, and S. Zapperi, Braz. J. Phys. **30**, 27 (2000).
- [23] R. Skoe, D. Vandembroucq, and S. Roux, Int. J. Mod. Phys. C **13**, 751 (2002).
- [24] D. Vandembroucq and S. Roux, preprint (2003).
- [25] L. Furuberg, J. Feder, A. Aharony, and T. Jossang, Phys. Rev. Lett. **61**, 2117 (1998).
- [26] S. Krishnamurthy, A. Tanguy, and S. Roux, Eur. Phys. J. B **15**, 149 (2000).
- [27] Z. Racz, in *Slow relaxations and nonequilibrium dynamics in condensed matter*, Les Houches Session LXXVII (EDP Sciences - Springer, 2002), pp. 1–40.
- [28] A. Rosso, W. Krauth, P. L. Doussal, K. Wiese, and J. Vannimenus, Phys. Rev. E **68**, 036128 (2003).
- [29] D. Vandembroucq, R. Skoe, and S. Roux, arXiv:cond-mat/0311485 (2003).
- [30] T. Antal, M. Droz, G. Gyorgy, and Z. Racz, Phys. Rev. E **65**, 046140 (2002).
- [31] Y. Charles, D. Vandembroucq, F. Hild, and S. Roux, accepted in J. Mech. Phys. Sol. (2003).